IEEE Access
Multidisciplinary ⋮ Rapid Review ⋮ Open Access Journal

Received 28 November 2024, accepted 17 December 2024, date of publication 25 December 2024,
date of current version 2 January 2025.

Digital Object Identifier 10.1109/ACCESS.2024.3522500

RESEARCH ARTICLE

Proposal and Simulation Analysis of Anchor-Less Cooperative Positioning Method Using Multiple Tags and Tag-Mounted Mobile Robot

MIREI YOSHIZAWA[1], TAKU SHIMIZU[1], AND SOUSUKE NAKAMURA[2], (Member, IEEE)
[1]Graduate School of Science and Engineering, Hosei University, Tokyo 184-8584, Japan
[2]Faculty of Science and Engineering, Hosei University, Tokyo 184-8584, Japan

Corresponding author: Mirei Yoshizawa (mirei.yoshizawa.3n@stu.hosei.ac.jp)

This work was supported by JSPS KAKENHI Grant Number JP24K15128.

ABSTRACT Ultra-wideband (UWB) positioning technology positions objects in environments where Global Navigation Satellite System (GNSS) signals are unavailable and is expected to be applied to a wide range of services. However, the challenges associated with anchor installation, such as the need for highly accurate manual positioning and the installation of many anchors, increase the effort and cost of system implementation. Therefore, this paper proposes an anchor-less tag positioning method based on the cooperative use of a mobile robot and multiple tags. This method uses a particle filter to integrate multiple distance measurements obtained via UWB and tag inertial information from Inertial Measurement Units (IMUs). The combination of tag self-calibration by the mobile robot and tag cooperative positioning using the distance between tags enables the omission of anchors. Simulation results show that the proposed method achieves positioning accuracy comparable to conventional anchor-based positioning systems.

INDEX TERMS Anchor-less, inertial measurement unit (IMU), indoor positioning system (IPS), particle filter (PF), sensor fusion, ultra-wideband (UWB).

I. INTRODUCTION

Indoor Positioning Systems (IPS) are used to locate objects in environments where Global Navigation Satellite System (GNSS) signals are unavailable [1]. This technology applies to various services, including inventory management in factories and warehouses, navigation for Automatic Guided Vehicles (AGV), positioning of mobile devices and IoT equipment, and route guidance in indoor facilities. Various methods have been proposed so far, including Wi-Fi, Bluetooth, Radio Frequency Identification (RFID), and Ultra-Wideband (UWB) [2], [3], [4]. Among them, positioning systems using UWB have attracted significant attention due to their high positioning accuracy, with positioning errors ranging from just a few centimeters to several tens of centimeters [5], [6], [7].

A typical UWB positioning system consists of two types of ranging devices: tags, which are the objects to be located, and anchors, which are fixed reference points in the environment. The standard approach involves measuring the distances between multiple pre-installed anchors and tags using UWB signals, followed by calculating the tag's position based on this distance information through techniques such as triangulation [8], [9], [10].

However, barriers to system implementation due to the installation of anchors have become an issue [11], [12], and research is underway to address this problem.

Firstly, high-precision anchor calibration requires manual effort. To solve this problem, researchers are conducting studies on the self-calibration of anchors using drones and Unmanned Aerial Vehicles (UAVs) equipped with Inertial Measurement Units (IMUs) [13], [14], [15]. In [13], real-time self-calibration of anchors was performed using the RANSAC paradigm based on the distances between the tag-mounted quadcopter and the anchors. In [14], anchor self-calibration was performed using a tightly-coupled Error-State Kalman Filter (ESKF) based on the distances between

The associate editor coordinating the review of this manuscript and approving it for publication was Dušan Grujić.

the tag-mounted UAV and the anchors and the UAV's IMU inertial measurements. In this way, mobile robots enable self-calibration of anchors without human intervention.

Moreover, the cost of anchor installation has increased due to the need to install many anchors and relocate them to appropriate positions. To solve this problem, researchers are conducting studies on collaborative localization using the distances between tags [12], [16], [17]. In [16], to avoid the reduction in range accuracy due to Non-Line-of-Sight (NLOS), some tags act as anchors and use Line-of-Sight (LOS) tag-to-tag distance information to improve positioning accuracy. This approach is expected to reduce the need for anchors and eliminate the hassle of relocating them. In [12], the authors suggest that collaborative localization of tags could theoretically eliminate the need for anchors. In [17], the relative positions of the tags were calculated by combining UWB ranging measurements between tags and IMU inertial measurements, without using anchors.

Additionally, in [18], [19], [20], [21], and [22], the positions of the tags are estimated by fusing UWB ranging measurements with IMU inertial measurements. In [18], more accurate positioning was achieved by fusing information using an Extended Kalman Filter (EKF), a type of Bayesian filter. Thus, the fusion of UWB and IMU information enables more accurate positioning.

Based on the above, this paper proposes a tag positioning method that eliminates the need for anchors by using a cooperative approach with a mobile robot and multiple tags. The method fuses multiple distance measurements from UWB and tags inertial information from IMU based on a particle filter [23]. This enables the omission of anchors by combining tag self-calibration using a mobile robot with collaborative localization among the tags. As a result, the barriers to the implementation of IPS are reduced.

The proposed method is helpful in scenarios where mobile robots are involved in tracking the positions of numerous objects. Representative applications include AGV transportation in warehouses, delivery or cleaning robots in facilities, and indoor applications such as smart furniture [24] or WPT robots [25]. In conventional anchor-based positioning systems, the installation of anchors on walls and the required power supply wiring posed challenges in terms of both installation costs and the appearance of the room. This method eliminates the need for anchors, resolving challenges related to high installation costs in large-scale environments and preserving the appearance of homes and offices.

The main contributions of this paper are as follows:

1) Using a mobile robot and multiple tags cooperatively, we propose a positioning method that does not require fixed anchors. Specifically, we achieve anchor-less positioning by fusing UWB distance information between a mobile robot and tags and between tags, together with IMU inertial information of the tag in a particle filter.

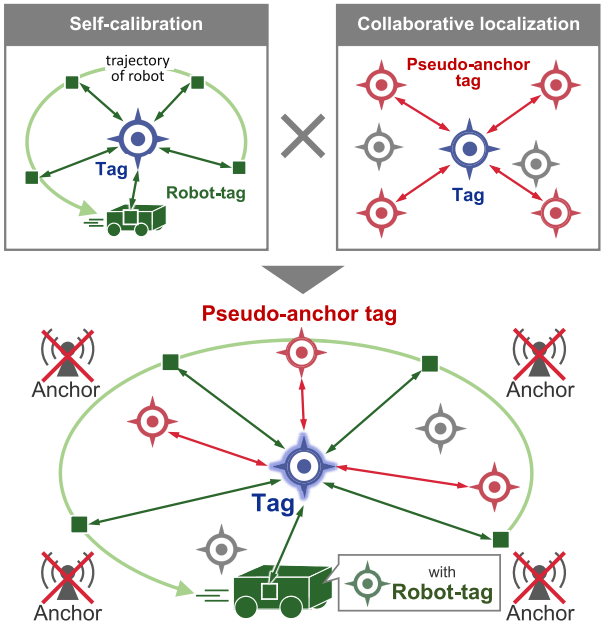

FIGURE 1. Anchor-less cooperative positioning method.

2) The performance of the proposed method was evaluated through simulations. Simulation results showed that the proposed algorithm achieves positioning accuracy comparable to conventional positioning systems using fixed anchors, although they are not required.

II. ANCHOR-LESS COOPERATIVE POSITIONING METHOD

A. METHOD OVERVIEW

In this paper, we propose a collaborative positioning algorithm that eliminates the need for anchors. The algorithm achieves localization by fusing distance measurements from UWB and inertial information from IMU with a particle filter. Fig. 1 shows a schematic diagram of the proposed method.

First, self-calibration of the tags is performed using a mobile robot. A tag is attached to the mobile robot, which moves within the environment while measuring distances to other tags. Based on the distance information and the robot's self-localization, the tag's position on the map is estimated.

Furthermore, if a tag has completed its position estimation and is stationary, it is used as a pseudo-anchor tag to support the cooperative position estimation of other tags. This pseudo-anchor tag functions similarly to a conventional anchor and measures distances to other tags. In other words, the position of tags is estimated using the pseudo-anchor tag's past estimated positions combined with distance information to other tags. In this paper, ''cooperation'' refers to mobile tags measuring distances to each other and collaboratively estimating their positions through mutual cooperation.

Additionally, the tag's inertial information obtained using an IMU is also utilized for position estimation.

By integrating these various pieces of information, each set complements the other, enabling tag positioning without the need for fixed anchors.

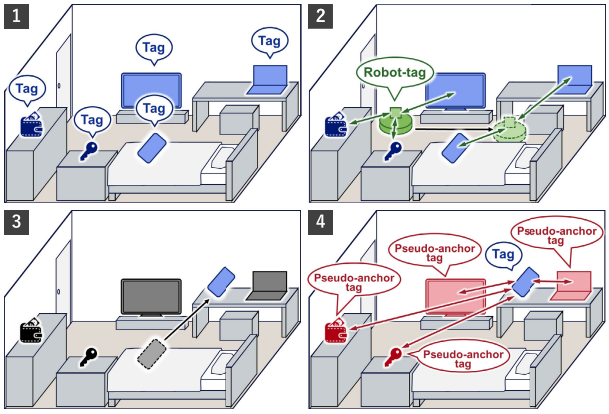

FIGURE 2. Application of Anchor-less cooperative positioning method in a Living Space.

We organize the terms used in this paper as follows:

- Anchor: A fixed device installed in the environment that serves as a reference point for position estimation. This paper aims to eliminate the use of anchors.
- Tag: A mobile device that serves as the target for position estimation.
- Robot-tag: A mobile device attached to a mobile robot. Its position is known and is used for the self-calibration of tags.
- Pseudo-anchor tag: A mobile device that has completed its position estimation and remains stationary. It serves as an anchor, supporting the collaborative position estimation of other tags. It serves both as a target for position estimation and as a reference point.

A practical application of the proposed method is illustrated in Fig. 2, depicting a scenario where multiple objects are localized within a living space. First, tags are attached to the objects that need to be localized (Step 1). Next, a mobile robot with a known position, equipped with a robot-tag, moves around the environment, measuring distances to the tags and estimating their positions (Step 2). Subsequently, if the target object moves (Step 3), stationary tags that were localized in Step 2 are used as reference points, conducting distance measurements and position estimation for the target (Step 4). The feature of this method is that tags, which are initially the targets of position estimation, can adaptively function as anchors, serving as positioning reference points, depending on their circumstances. This eliminates the need to install dedicated fixed anchors, allowing localization to be achieved using only tags. Another notable feature is that the tags collaborate to estimate their positions, so the mobile robot does not need to be present at all times.

B. SENSOR INFORMATION

The sensor information used for positioning consists of three types: two types of distance information from UWB and inertial information from IMU.

The first component is the UWB distance measurements to the pseudo-anchor tags (Fig. 1: red lines). A pseudo-anchor tag is a tag that plays the role of an anchor in a pseudo manner, remains stationary and has completed its position estimation. First, a tag is determined to be stationary if the change in its IMU measurements is below a certain threshold. Then, the tag is considered to have completed position estimation when the standard deviation of its estimated positions over the past n time steps, falls below the threshold. When a tag meets both conditions, it becomes a pseudo-anchor tag, serving as both a positioning target and a positioning reference point. This distance information and the position estimates of pseudo-anchor tags are used in the weight calculation of the PF. This approach eliminates the need for anchors and allows for positioning even when the mobile robot is not operating.

The second component is the UWB distance measurements to the robot-tag (Fig. 1: green lines). A robot-tag is a tag attached to a mobile robot, whose position is always known through self-localization techniques. The mobile robot with the robot-tag moves within the environment, continuously measure the distances to the tags. This distance information and the position of the robot-tag are used to calculate the weight in PF. However, the positions of the robot-tag and the mobile robot are obtained using established self-localization techniques such as Simultaneous Localization and Mapping (SLAM) or adaptive Monte Carlo localization (AMCL).

The third component is the inertial measurements of the tags obtained from the IMU. A 6-axis IMU attached to the tag captures the 3-axis acceleration and 3-axis angular velocity of the tag. The inertial information is used to estimate the tag's 3D position and orientation, which is used for state prediction in the PF. This inertial information helps maintain the tag's positioning accuracy even when the distance information is insufficient. This approach ensures that a certain level of positioning accuracy is maintained even when the mobile robot is not operating or the number of tags available for cooperative use is limited.

C. SENSOR MODELING

To simulate realistic sensor information, the sensors were modeled as follows.

The distance measurement $z(t)$ is defined as the true distance $z_G(t)$ with the addition of multiple noise components.

$$z(t) = z_G(t) + b_n(t) + b_z(t) \tag{1}$$

Here, $z_G(t)$ represents the true Euclidean distance to the target tag. Additionally, $b_n(t)$ is white noise following a normal distribution $\mathcal{N}(0, \sigma_z^2)$, and $b_z(t)$ is offset noise with a magnitude of σ_{z_o} that occurs with low probability due to factors such as multipath effects.

The inertial measurements $a_b(t)$ and $\omega_b(t)$ are defined as the true acceleration $a_G(t)$ and angular velocity $\omega_G(t)$ with the addition of multiple noise components.

$$a_b(t) = a_G(t) + b_{N_a}(t) + b_{B_a}(t) + b_{K_a}(t) \tag{2}$$

$$\omega_b(t) = \omega_G(t) + b_{N_\omega}(t) + b_{B_\omega}(t) + b_{K_\omega}(t) \tag{3}$$

The noise terms $b_{N_a}(t)$, $b_{N_\omega}(t)$, $b_{B_a}(t)$, $b_{B_\omega}(t)$, $b_{K_a}(t)$, $b_{K_\omega}(t)$ are defined based on [26]. Specifically, $b_{N_a}(t)$ and $b_{N_\omega}(t)$

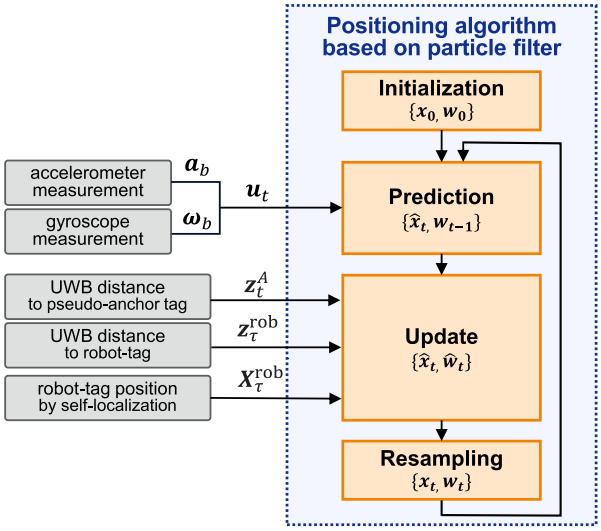

FIGURE 3. Positioning algorithm based on particle filter.

represent high-frequency random noise as white noise, defined using the power spectral density coefficients N_a and N_ω in (4). Similarly, $b_{B_a}(t)$ and $b_{B_\omega}(t)$ represent low-frequency variations over long durations as bias instability drift, defined using the coefficients B_a and B_ω in (5). Additionally, $b_{K_a}(t)$ and $b_{K_\omega}(t)$ represent the cumulative error growth as random walk drift, defined with the coefficients K_a and K_ω in (6). Here, $w(t)$ is white noise following the normal distribution $\mathcal{N}(0, 1)$ at time t, and f denotes the sampling rate.

$$b_N(t) = w(t) \cdot \sqrt{\frac{f}{2}} \cdot N \tag{4}$$

$$b_B(t) = 0.5 \cdot b_B(t-1) + w(t) \cdot B \tag{5}$$

$$b_K(t) = b_N(t-1) + w(t) \cdot \frac{K}{\sqrt{\frac{f}{2}}} \tag{6}$$

D. POSITIONING BASED ON PARTICLE FILTER

This method performs cooperative positioning by fusing multiple sensor data using a PF, a type of Bayesian filter. The main advantage of this filter is its ability to handle nonlinear models and multimodal observations. In indoor ranging, outliers and multimodal observations that do not follow a normal distribution may occur due to multipath. Therefore, this method uses a PF instead of a Kalman filter, which can only handle linear models.

This method predicts the state of particles using IMU inertial information and updates these predictions based on two types of UWB distance measurements.

III. POSITIONING ALGORITHM BASED ON PARTICLE FILTER

A. ALGORITHM OVERVIEW

This section gives an overview of the proposed algorithm based on PF. Fig. 3 shows the system diagram of the algorithm,

TABLE 1. Symbol definition.

Symbol	Definition
M	number of particles, $m = 1, \ldots, M$
$\boldsymbol{A}$	pseudo-anchor tags, $\boldsymbol{A} = \{A_1, A_2, \ldots, A_n\}$
$\boldsymbol{x}_t$	position of particles at time t
$\boldsymbol{x}_t^m$	position of mth particle at time t
$\hat{\boldsymbol{x}}_t$	position of particles at time t after prediction
$\hat{\boldsymbol{x}}_t^m$	position of mth particle at time t after prediction
$\boldsymbol{w}_t$	weight of particles at time t
w_t^m	weight of mth particle at time t
$\hat{\boldsymbol{w}}_t$	weight of particles at time t after update
$\hat{w}_t^m$	weight of mth particle at time t after update
$\boldsymbol{u}_t$	odometry at time t
$z_t^{A_i}$	distance data to pseudo-anchor tag A_i at time t
$\boldsymbol{z}_\tau^{\mathrm{rob}}$	distance data to robot-tag at time group $\boldsymbol{\tau}$
$\boldsymbol{X}_t^{A_i}$	estimated position of pseudo-anchor tag A_i at time t
$\boldsymbol{X}_\tau^{\mathrm{rob}}$	position of robot-tag at time group $\boldsymbol{\tau}$
$\boldsymbol{X}_t^{\mathrm{est}}$	position estimate at time t
$\boldsymbol{\tau}$	Set of times selected, $\boldsymbol{\tau} = \{\tau_1, \tau_2, \ldots, \tau_n\}$
$\boldsymbol{\epsilon_t}$	system noise at time t, following Gaussian distribution $\mathcal{N}(0, \sigma_Q^2)$
ν_t	observation noise at time t, following Gaussian distribution $\mathcal{N}(\mu_R, \sigma_R^2)$

Algorithm 1 Positioning Algorithm Based on Particle Filter

Input: $\boldsymbol{u}_{1:t}, \boldsymbol{z}_{1:t}^A, \boldsymbol{z}_{1:t}^{\mathrm{rob}}, \boldsymbol{X}_{1:t}^{\mathrm{rob}}$
Output: $\boldsymbol{X}_{1:t}^{\mathrm{est}}$

```
Generate initial particle set, χ_0 = {x_0, w_0}.
while positioning do
    for particle m = 1 to M do
        Predict Step:
            Update system noise parameter, σ_Q.
            Predict particle positions, x̂_t^m.
        Update Step:
            Judge pseudo-anchor tags, A.
            Update particle weights, ŵ_t^m.
    end for
    Resampling Step:
        Select estimated position, X_t^est.
        Generate new particle set, χ_t = {x_t, w_t}.
end while
```

Table 1 lists the definition of the variables, and Algorithm 1 presents the pseudocode.

This algorithm estimates the tag position $\boldsymbol{X}_t^{\mathrm{true}}$ at time t by iteratively performing observation, prediction, prediction update, and resampling based on the following components.

- $\chi_0 = \{\boldsymbol{x}_0, \boldsymbol{w}_0\}$: The initial state of the particles. The initial positions $\boldsymbol{x}_0$ are uniformly distributed across the entire environment, and the initial weights $\boldsymbol{w}_0$ are equal, given by $\boldsymbol{w}_0 = 1/M$.
- $\boldsymbol{u}_{1:t}$: The odometry up to time t obtained from the IMU.
- $\boldsymbol{z}_{1:t}^A$: The distance measurements between pseudo-anchor tags and tag up to time t obtained from the UWB.
- $\boldsymbol{z}_{1:t}^{\mathrm{rob}}$: The distance measurements between robot-tag and tag up to time t obtained from the UWB.
- $\boldsymbol{X}_{1:t}^{\mathrm{rob}}$: The robot-tag position up to time t.

B. PREDICTION

In the prediction step, the predicted position $\hat{\boldsymbol{x}}_t$ at time t is calculated using the particle position $\boldsymbol{x}_{t-1}$ at time $t-1$, the odometry $\boldsymbol{u}_t$ at time t, and the system noise ϵ_t.

The odometry $\boldsymbol{ut} = [u_{t_x}, u_{t_y}, u_{t_z}]^T$ represents the displacement of the object at time t, calculated from the measured accelerations and angular velocities. First, the current quaternion $q(t)$ is determined using the angular velocity $\omega_b(t)$ in the IMU coordinate frame at time t and the quaternion $q(t-1)$ at time $t-1$.

$$\begin{aligned}\omega_b(t) &= [0, \omega_{b_x}(t), \omega_{b_y}(t), \omega_{b_z}(t)]^T \\ q(t) &= [q_w(t), q_x(t), q_y(t), q_z(t)]^T \\ \dot{q}(t) &= \frac{1}{2} q(t-1) \otimes \omega_{\boldsymbol{b}}(t) \qquad (7) \\ q(t) &= q(t-1) + \int_{t-1}^{t} \dot{q}(\tau) d\tau \qquad (8)\end{aligned}$$

Next, the acceleration $\boldsymbol{a}_b(t)$ in the IMU coordinate frame at time t is transformed into the acceleration $\boldsymbol{a}_w(t)$ in the indoor positioning coordinate frame.

$$\begin{aligned}\boldsymbol{a}_b(t) &= [0, a_{b_x}(t), a_{b_y}(t), a_{b_z}(t)]^T \\ \boldsymbol{a}_w(t) &= [0, a_{w_x}(t), a_{w_y}(t), a_{w_z}(t)]^T \\ \boldsymbol{a}_w(t) &= q(t) \otimes \boldsymbol{a}_b(t) \otimes q(t)^{-1} \qquad (9)\end{aligned}$$

Then, using $\boldsymbol{a}_w(t)$ and the velocity $\boldsymbol{v}_w(t-1)$ in the indoor positioning coordinate frame at time $t-1$, the velocity $\boldsymbol{v}_w(t)$ is calculated according to (10).

$$\begin{aligned}\boldsymbol{v}_w(t) &= [v_{w_x}(t), v_{w_y}(t), v_{w_z}(t)]^T \\ \boldsymbol{v}_w(t) &= \boldsymbol{v}_w(t-1) + \int_{t-1}^{t} \boldsymbol{a}_w(\tau) d\tau \qquad (10)\end{aligned}$$

Finally, the position change $\boldsymbol{p}_w(t)\Delta t$ in the indoor positioning coordinate system is calculated using $\boldsymbol{v}_w(t)$ according to (11). The $\boldsymbol{p}_w(t)\Delta t$ represents the displacement at time t corresponding to the odometry $\boldsymbol{u}_t$.

$$\begin{aligned}\boldsymbol{p}_w(t) &= [p_{w_x}(t), p_{w_y}(t), p_{w_z}(t)]^T \\ \boldsymbol{u}_t &= \boldsymbol{p}_w(t)\Delta t = \int_{t-1}^{t} \boldsymbol{v}_w(\tau) d\tau \qquad (11)\end{aligned}$$

The system noise ϵ_t is a three-dimensional noise that follows a normal distribution with mean 0 and standard deviation σ_Q. The standard deviation σ_Q is dynamically updated based on the state of the target to improve positioning accuracy and prevent particle degeneration. Specifically, the state of the tag is determined based on past estimated positions $\boldsymbol{X}^{\text{est}}_{t-n:t-1}$ and $\boldsymbol{u}_t$. When the tag is moving or the position estimation is incomplete, σ_Q is set to a large value. Conversely, when the position estimation is determined to be complete, σ_Q is set to a small value.

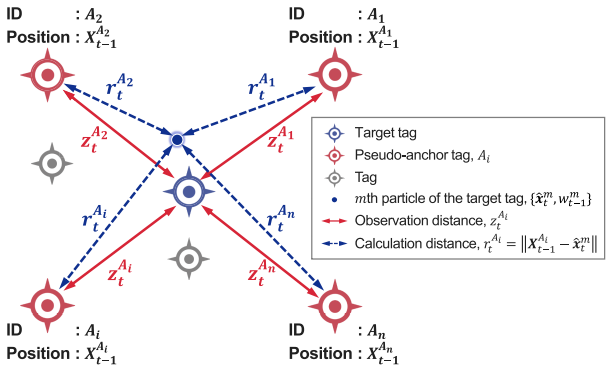

FIGURE 4. Likelihood by distance z_t^A.

Accordingly, the predicted position $\hat{\boldsymbol{x}}_t^m$ of particle m at time t is expressed by the following equation (12).

$$\begin{aligned}\hat{\boldsymbol{x}}_t^m &= \boldsymbol{x}_{t-1}^m + \boldsymbol{u}_t + \epsilon_t \\ &= \begin{bmatrix} x_{t-1}^m \\ y_{t-1}^m \\ z_{t-1}^m \end{bmatrix} + \begin{bmatrix} u_{t_x} \\ u_{t_y} \\ u_{t_z} \end{bmatrix} + \begin{bmatrix} \epsilon_{t_x} \\ \epsilon_{t_y} \\ \epsilon_{t_z} \end{bmatrix} = \begin{bmatrix} \hat{x}_t^m \\ \hat{y}_t^m \\ \hat{z}_t^m \end{bmatrix} \qquad (12)\end{aligned}$$

C. UPDATE

In the update step, the particle weights $\hat{\boldsymbol{w}}_t$ are calculated based on the predicted particle states $\{\hat{\boldsymbol{x}}_t, \boldsymbol{w}_{t-1}\}$ at time t, the ranging values z_t^A at time t, the estimated positions of pseudo-anchor tags $\boldsymbol{X}_{t-1}^A$ at time $t-1$, and the ranging measurements $\boldsymbol{z}_\tau^{\text{rob}}$ and robot-tag positions $\boldsymbol{X}_\tau^{\text{rob}}$ over past time steps τ. First, the likelihood $L(\hat{\boldsymbol{x}}_t^m \mid z_t^A)$ of particle m is computed based on the ranging measurements $\boldsymbol{z}_t^A$ with the pseudo-anchor tags, and the likelihood $L(\hat{\boldsymbol{x}}_t^m \mid \boldsymbol{z}_\tau^{\text{rob}})$ is computed based on the ranging measurements $\boldsymbol{z}_\tau^{\text{rob}}$ with the robot-tag. By integrating these likelihoods, the weight $\hat{\boldsymbol{w}}_t^m$ of particle m is determined.

1) DISTANCE TO PSEUDO-ANCHOR TAG

The likelihood $L(\hat{\boldsymbol{x}}_t^m \mid z_t^A)$ of the predicted position $\hat{\boldsymbol{x}}_t^m$ for particle m is calculated based on the distances $\boldsymbol{z}_t^A$ to all pseudo-anchor tags $\boldsymbol{A}$ at time t and the estimated positions $\boldsymbol{X}_{t-1}^A$ of all pseudo-anchor tags $\boldsymbol{A}$ at time $t-1$ (Fig. 4).

First, the pseudo-anchor tags $\boldsymbol{A} = A_1, A_2, \ldots, A_n$ are determined using the current odometry $\boldsymbol{u}_t$ and the estimated positions $X^{\text{est}}_{t-n:t-1}$ from the past n time steps. A pseudo-anchor tag is a tag that has been determined to be stationary and whose position has already been estimated. If a tag satisfies the two conditions in (13) and (14), this tag is identified as a pseudo-anchor tag.

$$\|\boldsymbol{u}_t\| < u_{\text{thres}} \text{ (m)} \qquad (13)$$

$$\|\sigma_{\boldsymbol{X}}\| < \sigma_{\text{thres}} \text{ (m)} \qquad (14)$$

In (13), the IMU measurements may include biases caused by offset drift, meaning the measured value might not be zero even when the tag is entirely stationary. Therefore, a tag is considered stationary only when $\|\boldsymbol{u}_t\|$ is below the threshold $u$thres. In (14), $\|\sigma_{\boldsymbol{X}}\|$ represents the norm of the standard

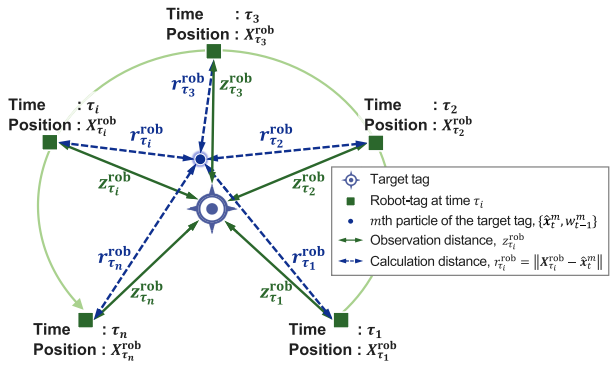

FIGURE 5. Likelihood by distance z^{rob}_{τ}.

deviation of $X^{\text{est}}_{t-n:t-1}$. If this value is below the threshold σ_{thres}, the position estimates are judged to have converged and stabilized, and the tag is regarded as having its position estimated.

The likelihood function for calculating the likelihood based on the ranging value $z^{A_i}_t$ to the pseudo-anchor tag A_i is given in (15). This likelihood function follows a normal distribution with mean $\mu_R = z^{A_i}_t$ and standard deviation σ_R.

$$L(\hat{\boldsymbol{x}}^m_t \mid z^{A_i}_t) = \frac{1}{\sqrt{2\pi}\sigma_R} \exp\left(-\frac{(r^{A_i}_t - z^{A_i}_t)^2}{2\sigma^2_R}\right) \tag{15}$$

Here, $r^{A_i}_t$ represents the Euclidean distance between the estimated position of the pseudo-anchor tag A_i, $\boldsymbol{X}^{A_i}_{t-1}$, and the predicted position of particle m, $\hat{\boldsymbol{x}}^m_t$, as defined in (16).

$$r^{A_i}_t = \|\boldsymbol{X}^{A_i}_{t-1} - \hat{\boldsymbol{x}}^m_t\| \tag{16}$$

At this point, since the pseudo-anchor tag remains stationary, the relationship $X^{A_i}_t = X^{A_i}_{t-1}$ holds. Consequently, in the likelihood calculation at time t, the estimated position $X^{A_i}_{t-1}$ from the previous time step can be utilized.

Then, as shown in Fig. 4, when multiple pseudo-anchor tags are present, the combined likelihood can be calculated using (17). Since each observation is independent, the combined likelihood is obtained by multiplying the likelihoods corresponding to each individual observation.

$$L(\hat{\boldsymbol{x}}^m_t \mid \boldsymbol{z}^A_t) = \prod_{i=1}^{n} L(\hat{\boldsymbol{x}}^m_t \mid z^{A_i}_t) \tag{17}$$

2) DISTANCE TO ROBOT-TAG

The likelihood $L(\hat{\boldsymbol{x}}^m_t \mid \boldsymbol{z}^{\text{rob}}_{\tau})$ of the predicted position $\hat{\boldsymbol{x}}^m_t$ for particle m is calculated based on the ranging values $\boldsymbol{z}^{\text{rob}}_{\tau}$ and the positions $\boldsymbol{X}^{\text{rob}}_{\tau}$ of the robot-tag at the set of time steps τ (Fig. 5).

The likelihood function for calculating the likelihood based on the ranging value $z^{\text{rob}}_{\tau_i}$ is given in (18). This likelihood function follows a normal distribution with a mean $\mu_R = z^{\text{rob}}_{\tau_i}$ and a standard deviation σ_R.

$$L(\hat{\boldsymbol{x}}^m_t \mid z^{\text{rob}}_{\tau_i}) = \frac{1}{\sqrt{2\pi}\sigma_R} \exp\left(-\frac{(r^{\text{rob}}_{\tau_i} - z^{\text{rob}}_{\tau_i})^2}{2\sigma^2_R}\right) \tag{18}$$

Here, $r^{\text{rob}}_{\tau_i}$ represents the Euclidean distance between the position of the robot-tag $\boldsymbol{X}^{\text{rob}}_{\tau_i}$ at time τ_i and the predicted position of particle m, $\hat{\boldsymbol{x}}^m_t$, as defined in (19).

$$r^{\text{rob}}_{\tau_i} = \|\boldsymbol{X}^{\text{rob}}_{\tau_i} - \hat{\boldsymbol{x}}^m_t\| \tag{19}$$

The set of time steps $\tau = \tau_1, \tau_2, \ldots, \tau_n$ is a set of times selected from the period $t_s : t$, where t_s is the time when the tag arrived at its current position (determined from the IMU data), and t is the current time. This indicates that the proposed method utilizes information obtained in the past for position estimation at time t. In conventional methods using fixed anchors, a sufficient number of anchors are appropriately placed to estimate the three-dimensional position (x, y, z). This allows multiple distance measurements from various directions to be obtained simultaneously at a single time step, making it possible to estimate the three-dimensional position using distance information from that single time step alone. On the other hand, in this method, as only a single robot is utilized, the robot-tag is limited to acquiring a single distance measurement from one direction at each time step. As a result, there is insufficient information to estimate the three-dimensional position with three degrees of freedom (x, y, z). To address this limitation, the proposed method leverages past distance and position information to enable three-dimensional position estimation.

Then, the likelihood that integrates all the information over the time set τ, including the past, can be calculated using (20). Since each observation is independent, the combined likelihood is obtained by multiplying the likelihoods corresponding to each individual observation.

$$L(\hat{\boldsymbol{x}}^m_t \mid \boldsymbol{z}^{\text{rob}}_{\tau}) = \prod_{i=1}^{n} L(\hat{\boldsymbol{x}}^m_t \mid z^{\text{rob}}_{\tau_i}) \tag{20}$$

At this point, all distance measurements $\boldsymbol{z}^{\text{rob}}_{t_s:t}$ and robot-tag positions $\boldsymbol{X}^{\text{rob}}_{t_s:t}$ acquired during the period $t_s : t$ can be used for weight calculation. However, as the operating time of the robot increases, the computational cost rises significantly, necessitating a restriction on the amount of information utilized. Therefore, as shown in Fig. 5, only the information obtained at the time steps $\tau = \tau_1, \tau_2, \ldots, \tau_n$, which are derived by dividing the period $t_s : t$ into $n - 1$ equal intervals, is utilized.

3) CALCULATION OF PARTICLE WEIGHTS

Finally, the particle weights $\hat{\boldsymbol{w}}^m_t$ that reflect all observations are calculated. Based on Bayes' theorem, the posterior probability can be obtained by multiplying the prior probability by the likelihood. Since the observations $\boldsymbol{z}^A_t$ and $\boldsymbol{z}^{\text{rob}}_{\tau}$ are uncorrelated and independent, the combined likelihood is the product of the individual likelihoods. Accordingly, the particle weights $\hat{\boldsymbol{w}}^m_t$ after incorporating the observations can be calculated using (21), based on the particle weights $\boldsymbol{w}^m_{t-1}$ before incorporating the observations and the observation likelihoods

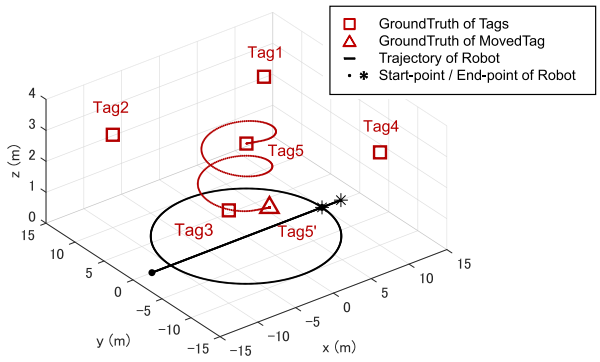

FIGURE 6. Simulation environment.

$L(\hat{\boldsymbol{x}}_t^m \mid \boldsymbol{z}_t^A)$ and $L(\hat{\boldsymbol{x}}_t^m \mid \boldsymbol{z}_\tau^{\text{rob}})$.

$$\hat{w}_t^m = w_{t-1}^m \times \underbrace{L(\hat{\boldsymbol{x}}_t^m \mid \boldsymbol{z}_t^A)}_{\text{Likelihood by } \boldsymbol{z}_t^A} \times \underbrace{L(\hat{\boldsymbol{x}}_t^m \mid \boldsymbol{z}_\tau^{\text{rob}})}_{\text{Likelihood by } \boldsymbol{z}_\tau^{\text{rob}}} \tag{21}$$

D. RESAMPLING

In the resampling step, a new set of particles $\chi_t = \{\boldsymbol{x}_t, \boldsymbol{w}_t\}$ is generated based on the particle states $\{\hat{\boldsymbol{x}}_t, \hat{\boldsymbol{w}}_t\}$ after incorporating the observations. This method employs systematic resampling [27]. Compared to simple resampling based on random numbers, systematic resampling is more effective in reducing computational costs and mitigating sampling bias.

In addition, before resampling, it is necessary to select the estimated position $\boldsymbol{X}_t^{\text{est}}$ as a representative value from the particle positions $\hat{\boldsymbol{x}}_t$. Since PF is an algorithm that estimates probability distributions, it is necessary to select a single point from the estimated probability distribution as the position estimate. In this method, the position of the particle with the maximum weight $\hat{w}_t^{\max}$ is adopted as the estimated position $\boldsymbol{X}_t^{\text{est}}$, using the maximum-weight approach. This approach has the advantage of reducing estimation errors in multipath environments, where the estimated distribution exhibits multimodality, compared to the commonly used weighted-average approach. The selected estimated position $\boldsymbol{X}_t^{\text{est}}$ is utilized as the position of the pseudo-anchor tag when the tag functions as a pseudo-anchor and is employed to estimate the positions of other tags.

Furthermore, this method incorporates a mechanism to suppress resampling during the initial stage of position estimation. At the start of position estimation, the tag's position information is not provided, and the information available for weight calculation is limited. As a result, it becomes difficult to uniquely identify particles close to the ground truth from those uniformly distributed throughout the environment, which may lead to divergence in the position estimation. To prevent this, the first resampling is performed when the maximum weight $\hat{w}_t^{\max}$ exceeds the threshold w_{thres}. The threshold w_{thres} is set to a value exceeding half of the total particle weights, considering that the sum of all particle weights is normalized to 1. This ensures that the particle most likely to be close to the ground truth is reliably selected, thereby reducing estimation errors during the initial stage of position estimation.

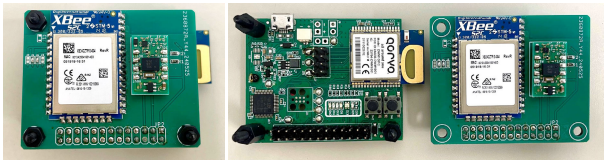

FIGURE 7. Appearance of the tag. (a) Top view of the tag. (b) Tag configuration: Qorvo's UWB module DWM1001-DEV (left) and BOSCH's IMU module BNO055 with XBee module (right), connected via pin headers.

TABLE 2. Noise parameters used for simulation.

	Parameter	Value	Unit
Range	σ_z	2.5×10^{-2}	m
	$\sigma_{z_{o_1}}$	3.0×10^{-2}	m
	$\sigma_{z_{o_2}}$	5.0×10^{-2}	m
Acceleration	N_a	2.3×10^{-3}	$(\text{m/s}^2)/\sqrt{\text{Hz}}$
	B_a	3.9×10^{-4}	m/s^2
	K_a	1.8×10^{-5}	$(\text{m/s}^2) \cdot \sqrt{\text{Hz}}$
Gyroscope	N_ω	2.4×10^{-4}	$(\text{rad/s})/\sqrt{\text{Hz}}$
	B_ω	7.7×10^{-6}	rad/s
	K_ω	2.6×10^{-7}	$(\text{rad/s}) \cdot \sqrt{\text{Hz}}$

IV. SIMULATIONS

A. SIMULATION CONDITION

A series of MATLAB simulations were performed to evaluate the effectiveness of the proposed method. As shown in Fig. 6, five tags (Tag1–Tag5) were placed in a 30 m × 30 m × 4 m simulation environment. The mobile robot and robot-tag moved on the x-y plane, and Tag5 was moved in a spiral motion to the position of Tag5'. The effectiveness of the proposed method was evaluated under different conditions by varying the trajectories of the robot-tag and Tag5 in each simulation.

The UWB distance measurements were performed at 10 Hz, the IMU inertial measurements at 50 Hz, and position estimation using these measurements was conducted at 10 Hz over a duration of 100 seconds. To simulate realistic sensor data, the UWB and IMU measurements were modeled using the characteristic parameters shown in Table 2. These parameters were identified from the actual measurement data of the tag shown in Fig. 7. For the UWB, σ_z was determined based on the standard deviation of the actual ranging measurement. Additionally, to simulate incidental noise caused by factors such as NLOS and multipath effects, offset noise $\sigma_{z_{o_1}}$ (with a 3% occurrence probability) and $\sigma_{z_{o_2}}$ (with a 1% occurrence probability) were introduced. Since this noise can vary significantly depending on environmental and situational factors, a simplified model was employed in this simulation. For the IMU, the parameters were identified using Allan variance analysis [28], [29] based on the actual inertial measurement. On the other hand, for simplicity, the position of the robot-tag was approximated using the true values without any noise.

TABLE 3. Position errors. (a) Cooperative positioning with robot-tag and pseudo-anchor tag and IMU. (b) Positioning with only robot-tag and IMU.

(a)

Tag	x-errors (m)	y-errors (m)	z-errors (m)	xyz-errors (m)
Tag1	0.019	0.016	0.050	0.061
Tag2	0.022	0.025	0.044	0.063
Tag3	0.020	0.023	0.044	0.060
Tag4	0.022	0.019	0.046	0.060
Tag5	0.015	0.015	0.036	0.046
Tag5'	0.017	0.025	0.074	0.087

(b)

Tag	x-errors (m)	y-errors (m)	z-errors (m)	xyz-errors (m)
Tag1	0.025	0.020	0.055	0.071
Tag2	0.020	0.024	0.049	0.066
Tag3	0.022	0.023	0.043	0.060
Tag4	0.027	0.018	0.045	0.062
Tag5	0.016	0.016	0.039	0.049
Tag5'	0.231	0.859	0.798	1.331

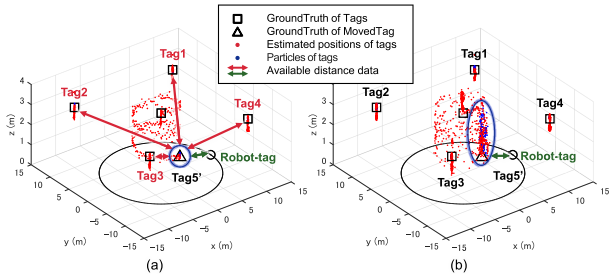

FIGURE 8. Position estimates and particles at 100 sec. (a) Cooperative positioning with robot-tag and pseudo-anchor tag and IMU. (b) Positioning with only robot-tag and IMU.

The simulations were repeated $k = 100$ times, and the position errors at time t were calculated as the mean Euclidean distance between the true value and the estimated position, as shown in (22).

$$\text{Position error (m)} = \frac{1}{k}\sum_{i=1}^{k} \|X_{t,i}^{\text{true}} - X_{t,i}^{\text{est}}\| \qquad (22)$$

In this simulation, the number of particles per tag was set to $M = 125$, uniformly distributed within the environment as a $5 \times 5 \times 5$ grid. The parameters were configured as follows: the threshold for determining whether the tag's position was estimated was $X_\sigma = 0.1$, the threshold for the first resampling was $w_{\text{thres}} = 0.7$, the standard deviation of system noise ranged from $\sigma_Q = 0.01$ to 0.10, and the standard deviation of observation noise was $\sigma_R = 0.10$. The value of σ_Q was initially set to 0.10, reduced to 0.02 after the first resampling, set to 0.05 during tag movement, and adjusted to 0.01 once position estimation was completed.

B. EVALUATION OF ANCHOR-LESS COOPERATIVE POSITIONING METHOD

To evaluate the effectiveness of the proposed method, two simulation results were compared: (a) positioning using the cooperative use of the robot-tag, pseudo-anchor tags, and IMU, and (b) positioning using only the robot-tag and IMU. The mobile robot moved in a counterclockwise circular path around the origin from 0 s to 50 s to avoid bias in each coordinate component of the distance information. Additionally, Tag5 moved in a spiral path from 50 s to 80 s after the mobile robot stopped.

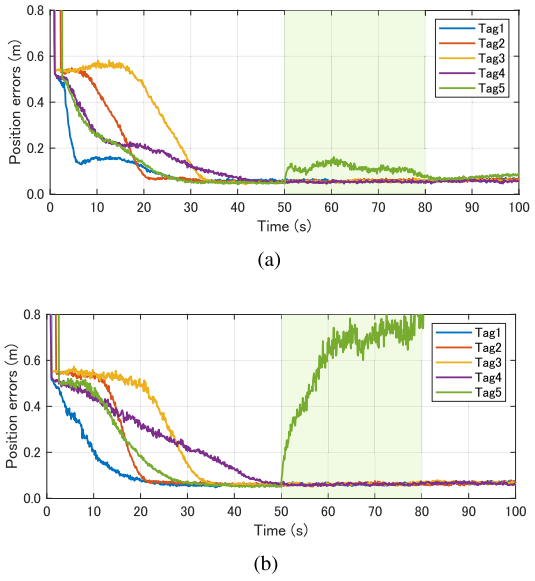

FIGURE 9. Time variation of position errors. (a) Cooperative positioning with robot-tag and pseudo-anchor tag and IMU. (b) Positioning with only robot-tag and IMU.

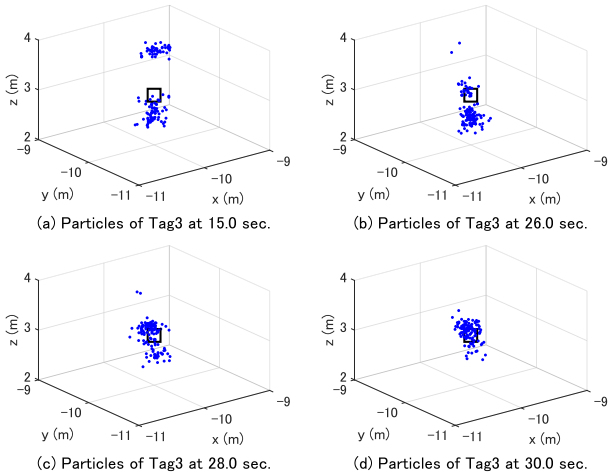

FIGURE 10. Multimodal distribution of particles due to ranging errors.

Table 3 shows the position errors for each tag along the coordinate axes, where the error for Tag5 corresponds to the value at 50 s, and the errors for Tag1—4 and Tag5' correspond to the values at 100 s. Fig. 8 shows the position estimations at 100 s. As shown in Table 3, the average position error in (a) was 0.058 m, demonstrating that the proposed method achieved positioning accuracy comparable to that of conventional UWB positioning systems. Additionally, regarding the positioning error of Tag5', it was significantly larger in (b) at 1.331 m, while it was much smaller in (a) at 0.087 m, indicating successful position estimation. This improvement is attributed

to the increased availability of distance information for particle weight calculation through pseudo-anchor tags. For $t > 50$ seconds, in (a), the weight calculation utilized not only IMU inertial information and distance information z_t^{rob} from the robot-tag (depicted by the green line in Fig. 8(a)), but also distance information $z_t^{\mathrm{Tag1}}, z_t^{\mathrm{Tag2}}, z_t^{\mathrm{Tag3}}, z_t^{\mathrm{Tag4}}$ from the pseudo-anchor tags (depicted by the red lines in Fig. 8(a)). In contrast, in (b), the weight calculation utilized only IMU inertial information and distance information z_t^{rob} from the robot-tag (depicted by the green line in Fig. 8(b)). Due to this difference, after Tag5 moved in (b), the particles failed to correctly track Tag5', leading to unsuccessful position estimation.

Furthermore, Fig. 9 shows the time variation in position errors for each tag. From this, it can be observed that (a) achieved a faster reduction in position errors and quicker convergence of position estimates compared to (b). This phenomenon is attributed to the pseudo-anchor tags improving the Dilution of Precision (DOP) [30], a positioning performance measure influenced by the robot's trajectory and tag placement. In (a), it is presumed that tags whose positions were quickly estimated acted as pseudo-anchor tags, thereby facilitating the position estimation of other tags. In particular, the pseudo-anchor tags are thought to have compensated for the lack of information in the z-axis component caused by the robot's position consistently being at $z = 0.0$ m. Furthermore, the average position error of Tag1—-Tag5 in (a) was 5.7% lower than in (b), which is also considered to result from the improvement in DOP.

Fig. 10 shows the particle distribution during the position estimation process for Tag3. This figure illustrates how particles transition from a multimodal distribution to a unimodal distribution as the estimation progresses. The proposed method is designed for scenarios where the initial positions of the tags are unknown and ranging errors caused by NLOS or multipath effects are likely to occur. Consequently, the particle distribution representing candidate position estimates may exhibit a multimodal pattern. Although a simplified noise model was employed in this simulation, it was confirmed that the method could proceed with position estimation without falling into local optima, even under such challenging conditions.

In conclusion, the proposed method demonstrated that it can achieve positioning accuracy comparable to conventional positioning methods, even without the need for fixed anchors. Furthermore, it was confirmed that cooperative interaction among multiple tags enables faster position estimation and reduces position errors. In addition, the method was shown to be capable of handling multimodal distributions caused by NLOS and multipath effects.

C. EVALUATION OF POSITIONING ACCURACY UNDER UNFAVORABLE TRAJECTORY OF ROBOT

Simulations with a modified robot trajectory were conducted to evaluate the effect of the robot trajectory on the proposed method. The mobile robot moved in a straight line from [-12.5, 0, 0] m to [12.5, 0, 0] m from 0s to 50s to intentionally introduce bias in each coordinate component of the distance information. Additionally, as in sec. IV-B, Tag5 moved in a spiral path from 50s to 80s.

TABLE 4. Position errors when the robot moved straight.

Tag	x-errors (m)	y-errors (m)	z-errors (m)	xyz-errors (m)
Tag1	0.019	9.223	0.350	9.395
Tag2	0.019	10.028	0.364	10.185
Tag3	0.022	9.433	0.340	9.601
Tag4	0.022	10.026	0.335	10.165
Tag5	0.015	0.310	0.047	0.319
Tag5'	0.096	0.521	0.474	0.804

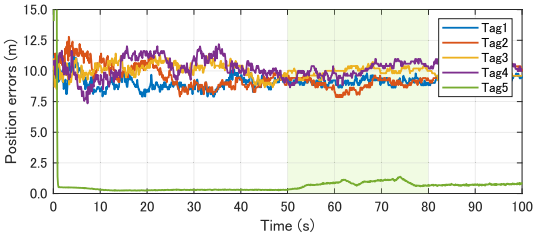

FIGURE 11. Time variation of position errors when the robot moved straight.

Table 4 shows the position errors of each tag for each coordinate axis, and Fig. 11 shows the time variation in position errors of each tag. From Table 4, it can be seen that the average position errors of Tag1–Tag4 is 10.105 m, which is significantly different from the ground truth. This is because, in the case of a symmetric trajectory for all tags, the distance information between each tag becomes equal, making it impossible to determine a unique position estimate. There are two reasons for this. First, when considering the distance information to the robot-tag, it is impossible to distinguish between two tags that always exist in a symmetrical positional relationship with respect to the robot trajectory. Second, when considering the distance information to pseudo-anchor tags, relative positional constraints among the tags can be constructed, but absolute constraints with respect to the map coordinate system are not feasible. As a result, it is assumed that the positions of Tag1 and Tag4, as well as Tag2 and Tag3, were mistaken for each other. The distance between the tags where such mispositioning occurred is 20 m, and the probability of this occurring is about 50%, resulting in position errors of about 10 m.

Therefore, it is clear that the mobile robot's trajectory and the tags' placement significantly affect the positioning accuracy of the proposed method.

D. EVALUATION OF POSITIONING ACCURACY AGAINST DIFFERENT TIMING OF TAG MOVEMENT

Simulations were conducted by varying the start time of Tag5's movement to evaluate the stability of the positioning. The

TABLE 5. Position errors when the tag's moving time changed.

time (s)	x-errors (m)	y-errors (m)	z-errors (m)	xyz-errors (m)
50 – 80	0.017	0.025	0.074	0.087
30 – 60	0.026	0.028	0.083	0.099
10 – 40	0.022	0.027	0.078	0.094
5 – 35	0.030	0.029	0.083	0.101
0 – 30	188.017	7.113	9.658	188.421

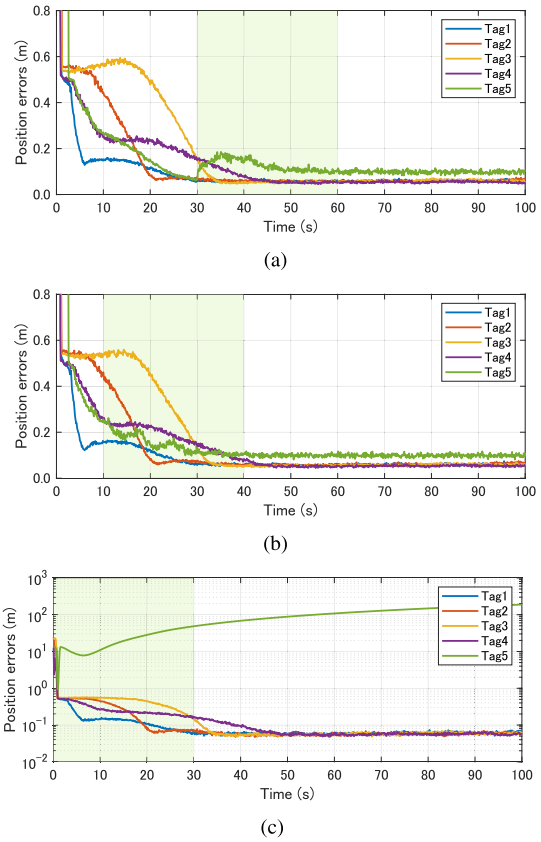

FIGURE 12. Time variation of position errors when the timing of Tag5's movement is varied. (a) Tag5 moved from 30 s to 60 s. (b) Tag5 moved from 10 s to 40 s. (c) Tag5 moved from 0 s to 30 s.

simulations were performed under three conditions: (a) Tag5 started moving at 30 s, when the positioning of all tags was almost complete; (b) Tag5 started moving at 10 s, when positioning was not yet complete after the first resampling; and (c) Tag5 started moving at 0 s, before the first resampling. Tag5 moved in a spiral path as described in sec. IV-B and IV-C. In addition, the mobile robot moved in a counterclockwise circular motion around the origin from 0 s to 50 s, as shown in sec. IV-B.

Table 5 shows the position errors of each tag for each coordinate axis, and Fig. 12 shows the time variation in the position errors of each tag. The results confirm that if the tags move after the first resampling, the final position errors remain largely unchanged. On the other hand, Fig. 12(c) shows that starting the tag's motion before the first resampling leads to larger position errors. This is likely because the tags move before particles close to the ground truth are selected from the uniformly distributed particles, causing the particles to diverge without converging.

In conclusion, it was demonstrated that the movement of the tags after the first resampling has minimal impact on the positioning accuracy.

V. CONCLUSION

In this paper, we proposed a tag positioning method that does not use anchors. This method employed the cooperative use of a mobile robot and multiple tags and IMU to overcome the limitations of installing anchor systems for UWB positioning systems. The simulation results confirmed that the combination of tag self-calibration by the mobile robot and cooperative localization among tags can eliminate the need for anchors. Additionally, we demonstrated that tag tracking is possible even when the mobile robot stops, achieving positioning accuracy equivalent to conventional UWB positioning systems, with errors below 0.10 m, except in certain limited situations.

In future work, practical experiments with actual devices will be necessary to validate the effectiveness of the proposed method in real-world environments. Moreover, since the noise model used in this simulation was partially simplified, further refinement of the algorithm will be required during real-world experiments. Additionally, the simulation results showed that the mobile robot's trajectory and the tags' placement affect the positioning accuracy. To address this issue, we plan to explore robot trajectory planning based on particle principal component analysis to enhance positioning accuracy.

REFERENCES

[1] F. Zafari, A. Gkelias, and K. K. Leung, "A survey of indoor localization systems and technologies," *IEEE Commun. Surveys Tuts.*, vol. 21, no. 3, pp. 2568–2599, 3rd Quart., 2019, doi: 10.1109/COMST.2019.2911558.

[2] R. Mautz, "Indoor positioning technologies," Ph.D. dissertation, Dept. Civil, Environ. Geomatic Eng., Inst. Geodesy Photogramm., ETH Zurich, Zrich, Switzerland, 2012.

[3] R. F. Brena, J. P. García-Vázquez, C. E. Galván-Tejada, D. Muñoz-Rodriguez, C. Vargas-Rosales, and J. Fangmeyer, "Evolution of indoor positioning technologies: A survey," *J. Sensors*, vol. 2017, pp. 1–21, Mar. 2017, doi: 10.1155/2017/2630413.

[4] P. S. Farahsari, A. Farahzadi, J. Rezazadeh, and A. Bagheri, "A survey on indoor positioning systems for IoT-based applications," *IEEE Internet Things J.*, vol. 9, no. 10, pp. 7680–7699, May 2022, doi: 10.1109/JIOT.2022.3149048.

[5] S. Gezici, Z. Tian, G. B. Giannakis, H. Kobayashi, A. F. Molisch, H. V. Poor, and Z. Sahinoglu, "Localization via ultra-wideband radios: A look at positioning aspects for future sensor networks," *IEEE Signal Process. Mag.*, vol. 22, no. 4, pp. 70–84, Jul. 2005, doi: 10.1109/MSP.2005.1458289.

[6] A. Alarifi, A. Al-Salman, M. Alsaleh, A. Alnafessah, S. Al-Hadhrami, M. Al-Ammar, and H. Al-Khalifa, "Ultra wideband indoor positioning technologies: Analysis and recent advances," *Sensors*, vol. 16, no. 5, p. 707, May 2016, doi: 10.3390/s16050707.

[7] W. Shule, C. M. Almansa, J. P. Queralta, Z. Zou, and T. Westerlund, "UWB-based localization for multi-UAV systems and collaborative heterogeneous multi-robot systems," in *Proc. Int. Conf. Future Netw. Commun. (FNC)*, vol. 175, Leuven, Belgium, Jan. 2020, pp. 357–364, doi: 10.1016/j.procs.2020.07.051.

[8] W. Wang, J. Huang, S. Cai, and J. Yang, "Design and implementation of synchronization-free TDOA localization system based on UWB," *Radioengineering*, vol. 27, no. 1, pp. 320–330, Apr. 2019, doi: 10.13164/re.2019.0320.

[9] I. Guvenc and C.-C. Chong, "A survey on TOA based wireless localization and NLOS mitigation techniques," *IEEE Commun. Surveys Tuts.*, vol. 11, no. 3, pp. 107–124, 3rd Quart., 2009, doi: 10.1109/SURV.2009.090308.

[10] Y. Qin, F. Wang, and C. Zhou, "A distributed UWB-based localization system in underground mines," *J. Netw.*, vol. 10, no. 3, pp. 134–140, Apr. 2015, doi: 10.4304/jnw.10.3.134-140.

[11] A. Albaidhani and A. Alsudani, "Anchor selection by geometric dilution of precision for an indoor positioning system using ultra-wide band technology," *IET Wireless Sensor Syst.*, vol. 11, no. 1, pp. 22–31, Feb. 2021, doi: 10.1049/wss2.12006.

[12] M. Ridolfi, A. Kaya, R. Berkvens, M. Weyn, W. Joseph, and E. D. Poorter, "Self-calibration and collaborative localization for UWB positioning systems: A survey and future research directions," *ACM Comput. Surveys*, vol. 54, no. 4, pp. 1–27, May 2021, doi: 10.1145/3448303.

[13] K. Batstone, M. Oskarsson, and K. Åström, "Towards real-time time-of-arrival self-calibration using ultra-wideband anchors," in *Proc. Int. Conf. Indoor Positioning Indoor Navigat. (IPIN)*, Sapporo, Japan, Sep. 2017, pp. 1–8, doi: 10.1109/IPIN.2017.8115885.

[14] Q. Shi, S. Zhao, X. Cui, M. Lu, and M. Jia, "Anchor self-localization algorithm based on UWB ranging and inertial measurements," *Tsinghua Sci. Technol.*, vol. 24, no. 6, pp. 728–737, Dec. 2019, doi: 10.26599/TST.2018.9010102.

[15] M. Hamer and R. D'Andrea, "Self-calibrating ultra-wideband network supporting multi-robot localization," *IEEE Access*, vol. 6, pp. 22292–22304, 2018, doi: 10.1109/ACCESS.2018.2829020.

[16] H. Cai, G. Wu, Y. Chen, and L. Jiang, "Indoor collaborative localization method based on ultra-wideband ranging," in *Proc. 9th Eur. Conf. Antennas Propag. (EuCAP)*, Lisbon, Portugal, Apr. 2015, pp. 1–2.

[17] R. Liu, C. Yuen, T.-N. Do, D. Jiao, X. Liu, and U.-X. Tan, "Cooperative relative positioning of mobile users by fusing IMU inertial and UWB ranging information," in *Proc. IEEE Int. Conf. Robot. Autom. (ICRA)*, Singapore, May 2017, pp. 5623–5629, doi: 10.1109/ICRA.2017.7989660.

[18] L. Yao, Y. A. Wu, L. Yao, and Z. Z. Liao, "An integrated IMU and UWB sensor based indoor positioning system," in *Proc. Int. Conf. Indoor Positioning Indoor Navigat. (IPIN)*, Sapporo, Japan, Sep. 2017, pp. 1–8, doi: 10.1109/IPIN.2017.8115911.

[19] W. You, F. Li, L. Liao, and M. Huang, "Data fusion of UWB and IMU based on unscented Kalman filter for indoor localization of quadrotor UAV," *IEEE Access*, vol. 8, pp. 64971–64981, 2020, doi: 10.1109/ACCESS.2020.2985053.

[20] S. O. H. Madgwick, A. J. L. Harrison, and R. Vaidyanathan, "Estimation of IMU and MARG orientation using a gradient descent algorithm," in *Proc. IEEE Int. Conf. Rehabil. Robot.*, Zurich, Switzerland, Jun. 2011, pp. 1–7, doi: 10.1109/ICORR.2011.5975346.

[21] M. Kok, J. D. Hol, and T. B. Schön, "Indoor positioning using ultrawideband and inertial measurements," *IEEE Trans. Veh. Technol.*, vol. 64, no. 4, pp. 1293–1303, Apr. 2015, doi: 10.1109/TVT.2015.2396640.

[22] A. Millane, H. Hesse, T. A. Wood, and R. S. Smith, "Range-inertial estimation for airborne wind energy," in *Proc. 54th IEEE Conf. Decis. Control (CDC)*, Osaka, Japan, Dec. 2015, pp. 455–460, doi: 10.1109/CDC.2015.7402242.

[23] P. M. Djuric, J. H. Kotecha, J. Zhang, Y. Huang, T. Ghirmai, M. F. Bugallo, and J. Miguez, "Particle filtering," *IEEE Signal Process. Mag.*, vol. 20, no. 5, pp. 19–38, Sep. 2003, doi: 10.1109/MSP.2003.1236770.

[24] O. Krejcar, P. Maresova, A. Selamat, F. J. Melero, S. Barakovic, and J. B. Husic, "Smart furniture as a component of a smart city—Definition based on key technologies specification," *IEEE Access*, vol. 7, pp. 94822–94839, 2019, doi: 10.1109/ACCESS.2019.2927778.

[25] S. Nakamura, T. Suzuki, Y. Kakinuma, S. Saruwatari, K. Yamamoto, K. Arai, K. Akiho, and H. Hashimoto, "Prototype system for energy management of mobile device via wireless charging robot," in *Proc. IEEE/ASME Int. Conf. Adv. Intell. Mechatronics (AIM)*, Jun. 2016, pp. 727–732, doi: 10.1109/AIM.2016.7576854.

[26] MathWorks. *ImuSensor—IMU Simulation Model*. MATLAB Documentation. Accessed: Nov. 25, 2024. [Online]. Available: https://www.mathworks.com/help/nav/ref/imusensor-system-object.html

[27] H. J. G. Gundersen and E. B. Jensen, "The efficiency of systematic sampling in stereology and its prediction," *J. Microsc.*, vol. 147, no. 3, pp. 229–263, Sep. 1987, doi: 10.1111/j.1365-2818.1987.tb02837.x.

[28] Y. Zhao, M. Horemuž, and L. E. Sjöberg, "Stochastic modelling and analysis of IMU sensor errors," *Arch. Photogramm., Cartography Remote Sens.*, vol. 22, pp. 437–449, Dec. 2011.

[29] X. Zhabg, Y. Li, and C. Rizos, "Allan variance analysis on error characters of MEMS inertial sensors for an FPGA-based GPS/INS system," in *Proc. Int. Symp. GPS/GNSS*, Tokyo, Japan, 2008, pp. 127–133.

[30] R. B. Langley, "Dilution of precision," *GPS World*, vol. 10, no. 5, pp. 52–59, 1999.

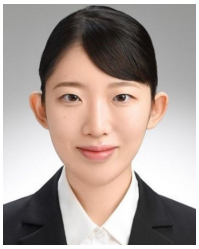

MIREI YOSHIZAWA received the B.E. degree in electrical and electronic engineering from Hosei University, Tokyo, Japan, in 2023, where she is currently pursuing the M.E. degree in electrical and electronic engineering. Her research interest includes indoor positioning with UWB for daily life application.

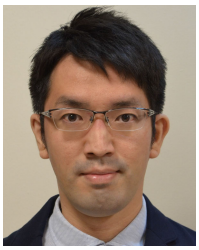

TAKU SHIMIZU received the B.E. and M.E. degrees in electrical engineering from the University of Tokyo, Japan, in 2011 and 2013 respectively. From 2013 to 2021, he was a Researcher with IHI Corporation. He joined Hitachi, Ltd., as a Researcher in 2021 where he is currently working as a Senior Researcher since 2023. He also joined Hosei University as a Project Researcher in 2019. His research interests include motion control, robotics and LiDAR-based recognition. He is a member of RSJ.

SOUSUKE NAKAMURA (Member, IEEE) received the B.E., M.E., and Dr.-Eng. degrees in electrical engineering from the University of Tokyo, Japan, in 2005, 2007, and 2012, respectively. From 2007 to 2009, he was an Engineer with Elysium Inc. In 2012, he joined Chuo University, as an Assistant Professor, and moved to Hosei University, where he has been a Professor, since 2023. His current research interests include assistive robotics, autonomous navigation, and power infrastructure, including wireless power transfer. He is a member of RSJ, SICE, IEEJ, JSME, and VRSJ.